

DuoSpaceNet: Leveraging Both Bird’s-Eye-View and Perspective View Representations for 3D Object Detection

Zhe Huang^{1,*} Yizhe Zhao^{2,*} Hao Xiao³ Chenyan Wu^{4,†} Lingting Ge²

¹Carnegie Mellon University ²University of California, San Diego

³University of Washington, Seattle ⁴The Pennsylvania State University

zhehuang@cmu.edu, yiz086@ucsd.edu, alexinu@uw.edu, czw390@psu.edu, gellingting@gmail.com

Abstract

Multi-view camera-only 3D object detection largely follows two primary paradigms: exploiting bird’s-eye-view (BEV) representations or focusing on perspective-view (PV) features, each with distinct advantages. Although several recent approaches explore combining BEV and PV, many rely on partial fusion or maintain separate detection heads. In this paper, we propose DuoSpaceNet, a novel framework that fully unifies BEV and PV feature spaces within a single detection pipeline for comprehensive 3D perception. Our design includes a decoder to integrate BEV–PV features into unified detection queries, as well as a feature enhancement strategy that enriches different feature representations. In addition, DuoSpaceNet can be extended to handle multi-frame inputs, enabling more robust temporal analysis. Extensive experiments on the nuScenes dataset show that DuoSpaceNet surpasses both BEV-based baselines (e.g., BEVFormer) and PV-based baselines (e.g., Sparse4D) in 3D object detection and BEV map segmentation, verifying the effectiveness of our proposed design.

1. Introduction

3D detection using multi-view images represents an active area of research [8–11, 18, 22–24, 27, 38, 47, 48, 54, 56], driven by critical applications in autonomous driving [12] where it substantially improves downstream tasks such as object tracking [17, 41] and motion prediction [4, 60, 61, 63]. Although LiDAR-based methods [3, 58, 59] often deliver superior performance for 3D detection, camera-only solutions provide distinct advantages: they are typically more cost-effective to deploy, perform reliably in adverse weather conditions such as rain or snow [62], and offer

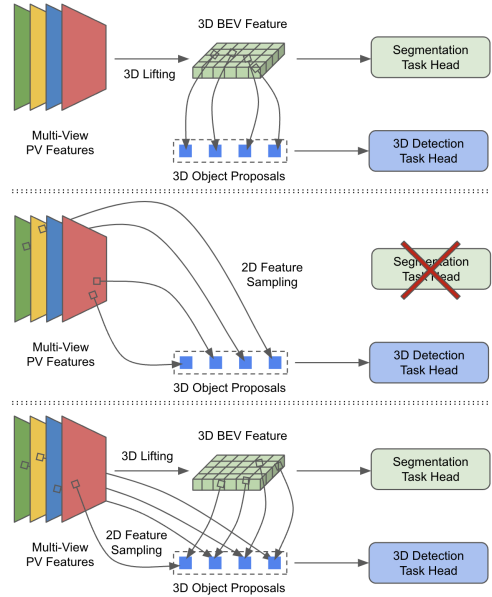


Figure 1. Comparison of different image-only 3D perception frameworks. (a) **Top:** Bird’s-eye-view-based (BEV-based) methods. (b) **Middle:** Perspective-view-based (PV-based) 3D detection-only methods. (c) **Bottom:** DuoSpaceNet (ours) where 3D detection benefits from both 3D BEV and 2D PV feature space.

higher resolution at greater distances with long focal length.

Most existing multi-view camera-only 3D object detection methods [5, 18, 21, 27, 48] fall into two broad categories: *bird’s-eye-view*-based (BEV-based) and *perspective-view*-based (PV-based), as illustrated in Fig. 1. BEV-based methods [5, 18] generate a bird’s-eye-view feature map through a 2D-to-3D lifting process—often leveraging camera projection or unprojection—where each element of the BEV map corresponds to a specific 3D location. Conversely, PV-based methods [21, 48] construct 3D detection heads atop 2D image features, typically relying on a limited set of sparse detection proposals. Visual cues are derived from the sparse feature locations where these pro-

*Equal contribution. †Corresponding author. This work was done at TuSimple (now CreateAI).

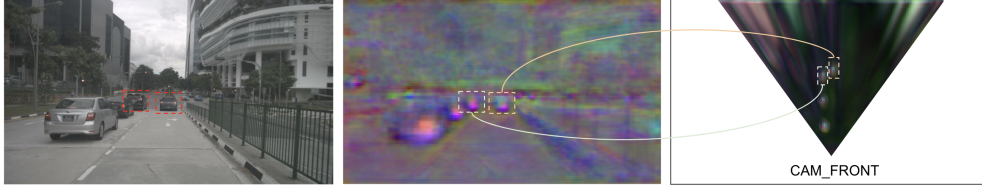


Figure 2. **Comparison of bird’s-eye-view (BEV) and perspective-view (PV) features.** (a) **Left:** The original front-facing RGB image. (b) **Middle:** PV heatmap. (c) **Right:** BEV heatmap. Both heatmaps are produced by our final model. Different hues and brightness levels represent various response intensities with black indicating minimal or no response. We highlight two car instances, each shown with its original image patch as well as corresponding PV and BEV heatmaps. The BEV heatmap in (c) makes it easier to interpret 3D positions—for instance, the relative positions of leading vehicles—without overlap issues. In contrast, the PV heat map in (b) preserves finer semantic details at higher resolution, which benefits attribute prediction.

posals are anchored. In general, PV-based methods prioritize object detection efficiency and computational speed.

While both BEV-based and PV-based methods can be effective, each exhibits notable limitations. In BEV-based methods, multi-view pose parameters guide the feature-lifting process, enhancing 3D geometric awareness and ensuring robustness to object-scale variations. They also avoid overlap artifacts arising from perspective projection. However, subtle visual cues can be lost due to coarse grid resolutions or interpolation. Moreover, the fixed-size nature of the BEV feature map discards objects outside its predefined coverage, even if they are rapidly approaching the ego-vehicle. By contrast, PV-based methods often maximize efficiency by sparsely attending to 2D PV features, allowing for theoretical detection at any distance. Yet, these methods typically rely on implicitly inferring 3D cues from 2D features, leading to weaker 3D perception. As shown in Fig. 2, retrieving spatial information from PV features is more difficult because of occlusion and perspective distortion, whereas BEV provides an unobstructed, rectified view. Still, BEV maps may omit fine-grained details for small objects (e.g., pedestrians or cyclists) and are subject to camera ray-like artifacts and limited coverage—issues that PV features do not face.

Some methods have attempted partial fusion of BEV and PV representations, yet they often depend on separate detection heads or derive visual cues predominantly from PV features. For example, BEVFormerv2 [57] combines BEV and PV features but maintains distinct detection heads, while the PETR series [26, 28] focuses on integrating BEV positional encodings into PV features. These partial approaches underscore the need for a more holistic solution to fully harness the complementary strengths of BEV and PV.

We introduce *DuoSpaceNet*, a holistic 3D perception framework that bridges the gap between bird’s-eye-view (BEV) and perspective-view (PV) approaches by leveraging both representations for 3D object detection and map segmentation. The core novelty of DuoSpaceNet is its truly integrated dual-space (also written as duo space) representation, where each object query contains both BEV and PV embeddings. Unlike systems that merely combine features

from separate heads, our method preserves the distinctiveness of each representation while merging them in a single, unified decoder for robust 3D perception.

Our architecture retains BEV and PV features and processes them with the *Duo Space Decoder*—a modified version of the transformer decoder from Deformable DETR. Each object query includes dual content embeddings from both spaces, along with a shared pose embedding representing the object’s real-world 3D position. Within the decoder, space-specific cross-attention layers refine dual-space object queries, enabling synergy between geometric and semantic cues. We further propose a feature divergence enhancement that maximizes the distinctiveness of BEV and PV features, leading to more discriminative representations.

Beyond single-frame detection, DuoSpaceNet supports a temporal extension that elegantly infuses multi-frame inputs into temporal queries, demonstrating our framework’s adaptability. For map segmentation, we append a segmentation head after BEV feature generation, with separate channels for each map category. By fusing both geometric and semantic insights in a single pipeline, DuoSpaceNet offers a comprehensive solution for multi-task 3D perception, setting it apart from existing methods that rely on partial fusion or separate detection heads.

Our main contributions are as follows:

- *Integrated Duo Space Framework:* We present *DuoSpaceNet*, which unifies BEV and PV representations within a single detection pipeline. This design features a *duo space decoder* for comprehensive BEV–PV fusion and a *divergence feature enhancement* technique that preserves the strengths of each view while enriching the combined representation.
- *Temporal Extension:* Our method also extends to temporal dimension with motion-compensated temporal queries, assisting 3D detection with multi-frame context.
- *Empirical Validation on nuScenes:* Through extensive experiments on the nuScenes [1] dataset, DuoSpaceNet outperforms both PV-only and BEV-only baselines, as well as other strong methods, in 3D detection and segmentation. Ablation studies further confirm the effectiveness of each proposed component.

2. Related Work

2.1. BEV-Based Multi-View 3D Perception

Tackling multi-view 3D object detection using bird’s-eye-view (BEV) representations has become popular in autonomous driving. Methods like LSS [37], BEVDet [9, 10], and BEVDepth [16] project 2D image features into BEV feature maps using dense depth predictions. M²BEV [54] and SimpleBEV [6] enhance efficiency by assuming uniform depth during back-projection. Notably, BEV methods such as BEVFormer series [18, 38, 56] avoid dense depth estimation by modeling BEV features with dataset-specific queries via deformable attention [68]. BEVFormer v2 [56] incorporates an auxiliary 3D detection head, while OCBEV [38] focuses on instance-level temporal fusion. Recent methods [5, 34, 35, 69] primarily improve temporal modeling rather than fundamental BEV representations.

BEV-based methods also address map segmentation tasks. VED [31] uses a variational encoder-decoder to generate BEV features, and VPN [33] employs an MLP-based transformation. Transformer-based approaches [36, 65] utilize cross-attention mechanisms to produce BEV representations. Recent geometric reasoning methods such as LSS [37] explicitly estimate depth distributions, while methods like M²BEV and BEVFormer leverage camera parameters and multi-task learning for enhanced detection and segmentation performance.

2.2. PV-Based Multi-View 3D Perception

Starting with DETR3D [48], the landscape of multi-view perspective-view-based (PV-based) 3D object detection leans towards sparse query refinement with set-to-set matching loss. Following studies like PETR [26, 27] and CAPE [55] improve transformer-based detection decoders with 3D position-aware image features. Recently, Sparse4D [21] further extends this track with the introduction of 4D anchors, allowing intuitive ego-motion and object motion compensation. We also find it useful and derive our query design from it. Similar to the BEV-based 3D detection track, current state-of-the-art PV-based methods, such as [22, 24, 47], also focus on improving temporal modeling techniques by temporal query propagation.

2.3. Unifying BEV and PV Detection

While several approaches have explored the fusion of Bird’s-Eye-View (BEV) and Perspective-View (PV) features for 3D detection, our proposed method stands apart by employing a fully shared detection head. BEVFormerv2 [57] pioneered the combination of BEV and PV queries to enhance BEV detection performance, but maintains separate detection heads for BEV and PV tasks. Furthermore, their detection queries contain either PV or BEV latent features exclusively, rather than integrating both. The PETR

series [26, 28] and StreamPETR [46] represent an alternative approach utilizing 3D queries and 2D PV features to detect 3D objects. However, these methods differ fundamentally from our work as their 3D queries contain only position embeddings, with all visual information derived solely from 3D PV image features. In contrast, our 2D-3D fused queries explicitly generate and incorporate BEV features, obtaining more comprehensive cues from both feature representations. MVF [66] presents perhaps the closest parallel to our approach, proposing a LiDAR-based 3D detection pipeline that leverages features from both 3D BEV space and 2D range image space. However, their method does not naturally extend to query-based camera-only detection systems like ours.

3. Method

As shown in Fig. 3, in our framework, PV and BEV feature maps are firstly generated from multi-view images and are then fed into the duo space decoder for object detection. The object queries equipped with duo space embedding are updated layer-by-layer in the decoder and the outputs from the last layer are used for predicting object labels and 3D poses. In addition, a dense segmentation head is built upon the BEV feature map for map segmentation.

3.1. Duo Space Features

Feature extraction. Multi-view images are first processed by an image encoder, which includes a backbone network (e.g., ResNet [7]) and a neck (e.g., FPN [19]), to generate multi-scale PV features $\{F_{PV}^j \in \mathbb{R}^{N \times C_j \times H_j \times W_j}, j = 1, 2, \dots, M\}$, where N, M are the number of cameras and different scales, H_j, W_j, C_j denote the feature map height, width and channel number of the j -th scale. Multi-view multi-scale PV features are lifted from 2D to 3D via a simple parameter-free back-projection module following previous work [6]. A 3D volume of coordinates with size $X \times Y \times Z$ is first generated and projected onto multiple images. PV features sampled around the projected positions are then aggregated by bilinear interpolation, resulting in a voxel feature map $F_{voxel} \in \mathbb{R}^{C \times X \times Y \times Z}$, where X, Y, Z, C represent the size of the voxel space and channels of the voxel feature. Eventually, the Z dimension is reduced to yield a BEV feature map $F_{BEV} \in \mathbb{R}^{C \times X \times Y}$.

In multi-frame settings, historical images are processed by the same procedure sequentially, generating PV and BEV feature maps for different frames. Both feature maps within a fixed temporal length are stored for future use.

Feature divergence enhancement. Our model benefits from the contrastiveness between the two feature representations. Since our lifting method is parameter-free, its functionality can be viewed as rearranging PV features given priors (e.g., camera poses) on the 3D geometry of a scene.

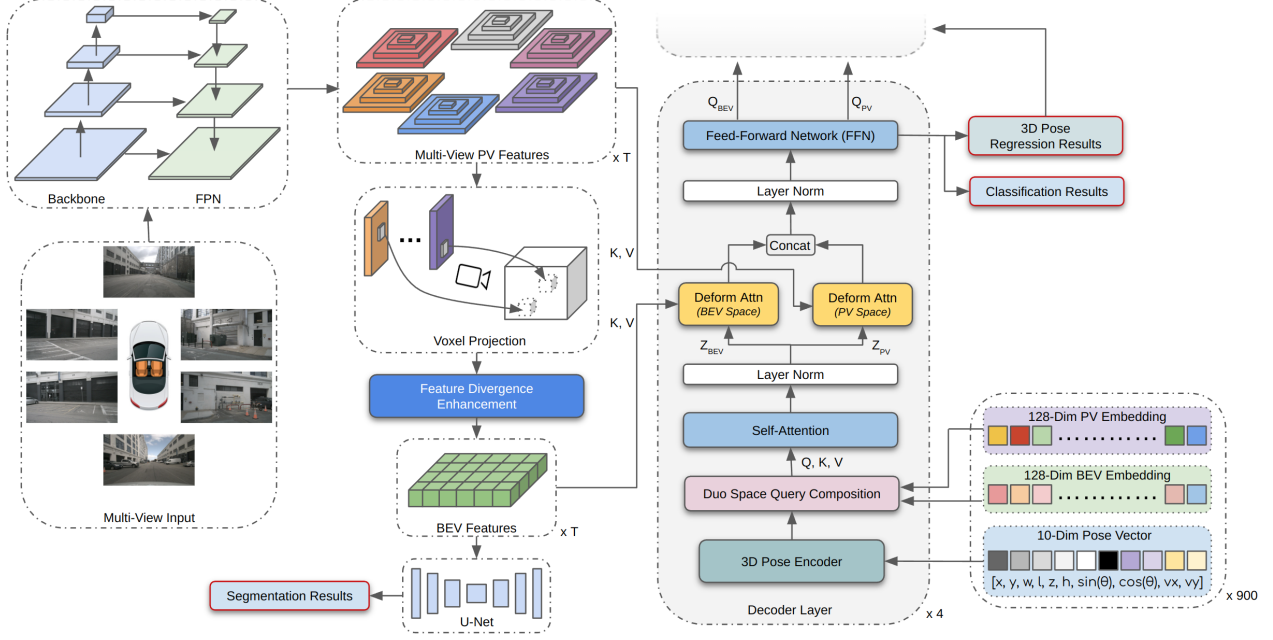


Figure 3. Overall architecture of the proposed DuoSpaceNet. Multi-view 2D perspective view (PV) features are extracted by the backbone and the feature pyramid network (FPN) [19]. Our 2D to 3D BEV lifting strategy consists of a parameter-free voxel projection following [6] and a divergence enhancement process to make resulting BEV features more distinctive w.r.t. PV features. In our duo space framework, multi-view PV features and BEV features are identified as equally important and are fed into the decoder together. Each decoder layer has one self-attention layer and two deformable cross-attention layers [68]. The self-attention layer acts on both BEV and PV spaces, whereas each cross-attention layer only attends to either BEV features or PV features. This space-specific cross-attention helps preserve the uniqueness of different feature spaces throughout multi-layer refinement process. Details about the Duo Space Query Composition can be found in Eqs. (2) to (4). Dense map segmentation can be jointly carried out via a separate segmentation head.

Therefore, it has minimal effects on diverging the feature contents. To increase the heterogeneity of BEV features w.r.t. PV features, we propose a simple yet effective divergence enhancement stage.

It consists of three 3D convolution layers (Conv3Ds) and three 2D convolution layers (Conv2Ds). First, we apply Conv3Ds on F_{voxel} to improve 3D geometry awareness in a learning-based fashion. After F_{voxel} is flattened along its Z dimension, Conv2Ds are applied for further BEV-level refinement, yielding final F_{BEV} .

3.2. Duo Space Decoder

Duo space queries. Suppose we have k object queries, $\{Q^i\}_{i=1}^k$. Each consists of a pose embedding, Q_{Pose}^i , and duo space content embedding for both BEV and PV spaces, Q_{BEV}^i and Q_{PV}^i , respectively.

Adapted from [21], each Q_{Pose}^i is encoded from a 3D pose vector \mathcal{P}_i , which contains attributes with physical meanings, including x, y, z in the vehicle coordinate system, the width, length, height, orientation and the velocity of the object the query is associated with. While Q_{BEV}^i and Q_{PV}^i contain high-level content features in BEV space and PV space respectively. In each layer of the duo space decoder, first, a pose encoder consisting of several FC layers is used to encode $\{\mathcal{P}_i\}_{i=1}^k$ into high dimensional latent representations, dubbed $\{\text{Enc}(\mathcal{P}_i)\}_{i=1}^k$, which will serve as

learnable positional encodings in the subsequent attention layers.

To unify the 3D pose of each object query across BEV and PV spaces, we generate a shared pose embedding,

$$Q_{Pose}^i = \xi(\text{Enc}(\mathcal{P}_i)), i \in \{1, 2, \dots, k\}, \quad (1)$$

where $\xi(\cdot)$ denotes a linear transformation to make the dimension of $\text{Enc}(\mathcal{P}_i)$ the same as Q_{BEV}^i and Q_{PV}^i . The final duo space queries in BEV space and PV space can be derived by simply adding the corresponding content embedding with the shared pose embedding together by

$$\mathbf{z}_{BEV} = \{Q_{BEV}^i + Q_{Pose}^i\}_{i=1}^k, \quad (2)$$

$$\mathbf{z}_{PV} = \{Q_{PV}^i + Q_{Pose}^i\}_{i=1}^k. \quad (3)$$

The self-attention layer thus can be represented as

$$Q = K = V = \mathbf{z}_{BEV} \oplus \mathbf{z}_{PV}, \quad (4)$$

$$\text{MHSA}(Q, K, V) = \text{Softmax}\left(\frac{QK^T}{\sqrt{\dim(K)}}\right)V, \quad (5)$$

where \oplus denotes a concatenation operator along the channel dimension and $\text{MHSA}(\dots)$ stands for multi-head self-attention described in [42].

Space-specific cross-attention. For multi-head cross-attention layers $\text{MHCA}_{BEV}(\dots)$ and $\text{MHCA}_{PV}(\dots)$, each of them will only act on their corresponding features using corresponding inputs.

In BEV space, it can be represented as

$$\hat{\mathbf{p}}_{BEV} = \{\mathcal{P}_i|_{x,y}\}_{i=1}^k, \quad (6)$$

$$\text{MHCA}_{BEV}(\dots) = \text{MSDA}(\mathbf{z}_{BEV}, \hat{\mathbf{p}}_{BEV}, F_{BEV}), \quad (7)$$

where $\hat{\mathbf{p}}_{BEV}$ denotes the normalized coordinates of 3D reference points (only using their X and Y components here). $\text{MSDA}(\dots)$ is the Multi-Scale Deformable Attention Module (MSDeformAttn) described in [68]. Similarly, we have cross-attention in PV space as

$$\hat{\mathbf{p}}_{PV} = \{\text{Proj}(\mathcal{P}_i|_{x,y,z}, \{\mathbf{K}_n, \mathbf{T}_n\}_{n=1}^N)\}_{i=1}^k, \quad (8)$$

$$\text{MHCA}_{PV}(\dots) = \text{MSDA}(\mathbf{z}_{PV}, \hat{\mathbf{p}}_{PV}, \{F_{PV}^j\}_{j=1}^M), \quad (9)$$

where $\text{Proj}(\dots)$ refers to the projection of 3D LiDAR coordinates into 2D image frames using camera matrices $\{\mathbf{K}_n\}_{n=1}^N \subset \mathbb{R}^{3 \times 3}$ and $\{\mathbf{T}_n\}_{n=1}^N \subset \mathbb{R}^{4 \times 4}$. Since this attention happens in PV space, multi-scale PV features $\{F_{PV}^j\}_{j=1}^M$ are used. Following feature extraction and refinement through multi-head space-specific cross-attention layers, the outputs of MHCA_{BEV} and MHCA_{PV} are concatenated as refined object queries, which are then fed into a 2-layer feed forward network (FFN). Finally, the FFN outputs are used for object category prediction and are also decoded into a 10-dim 3D pose vector as our detection regression results. The refined poses then serve as inputs for subsequent decoder layers.

3.3. Duo Space Temporal Modeling

BEV-based 3D detection methods [9, 18] typically utilize temporal inputs by stacking temporal BEV feature maps. Offsets are determined either with motion compensation or in a learnable manner (e.g., deformable attention) or both combined. Meanwhile, PV-based methods [21, 27] generally infuse temporal information into object queries. Therefore, the difference between BEV-based and PV-based temporal methods brings challenges to temporal design in our duo space paradigm. In this section, we present a unified temporal solution for both spaces via temporal duo space queries, illustrated in Fig. 4. Concretely, for a fixed temporal length l , each object is represented by l temporal duo space queries, each comprising a temporal pose of the underlying object and a shared content embedding. Temporal poses are deduced by applying both ego- and object-motion compensation on the object’s current pose vector.

The queries are fed into the space-specific cross-attention layer corresponding to their space. Each query only attends to features from a specific timestamp associated with its temporal pose. Subsequently, results produced by l temporal queries are recurrently aggregated via

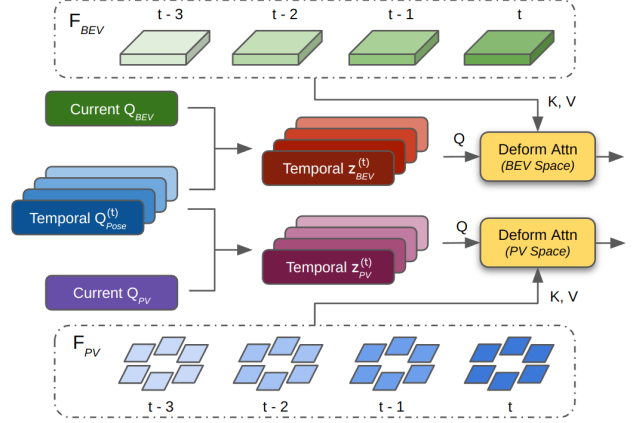


Figure 4. Diagram of the proposed duo space temporal modeling with 4 frames. Temporal pose embeddings $Q_{Pose}^{(t)}$ are generated by warping pose vectors at current timestamp through motion compensation. Subsequently, temporal duo space queries $\mathbf{z}_{BEV}^{(t)}$ and $\mathbf{z}_{PV}^{(t)}$ are assembled by broadcasting current content embeddings over the time dimension and then combining them with the temporal pose embeddings. We then conduct space-specific cross-attention using recent BEV and PV feature maps, both of which are maintained by their respective memory queue. Note that temporal queries from each timestamp only interact with feature maps corresponding to that timestamp. The resulting temporal queries are aggregated via a MLP in a recurrent fashion.

multi-layer perceptron (MLP) into a single refined prediction per object. Our solution elegantly operates symmetrically across BEV and PV spaces. Please refer to the supplementary materials for more details.

3.4. Multi-Task Learning

Similar to BEV-based methods, our model is capable of joint optimization of detection and segmentation. To perform dense segmentation, we simply add a segmentation branch consisting of a U-Net [39] like structure for feature enhancement and two parallel convolution-based segmentation heads for final predictions. It takes the BEV feature map F_{BEV} as input, and outputs two segmentation masks of the same resolution. To supervise the map segmentation branch, we use a weighted sum of focal loss [20] and dice loss [32] during training.

4. Experiments

Dataset. We benchmark our method on nuScenes dataset [1], one of the most widely-used public datasets in autonomous driving. The nuScenes dataset consists of 1,000 driving video clips. Each clip is 20-second long at the sampling frequency of 2Hz. Across the dataset, image data come from the same 6-camera setup, facing at 6 directions, providing a full 360° panoramic view. For 3D object detection task, the dataset contains 10 commonly-seen classes (e.g., car, pedestrian), in total $\sim 1.4\text{M}$ bounding boxes. We evaluate our 3D detection results using official nuScenes metrics, including mean average preci-

Method	Image Size	Frames	mAP \uparrow	NDS \uparrow	mATE \downarrow	mASE \downarrow	mAOE \downarrow	mAVE \downarrow	mAAE \downarrow
DETR3D [48]	1600 \times 900	1	0.349	0.434	0.716	0.268	0.379	0.842	0.200
PETR [26]	1600 \times 900	1	0.370	0.442	0.711	0.267	0.383	0.865	0.201
BEVFormer-S [18]	1600 \times 900	1	0.375	0.448	0.725	0.272	0.391	0.802	0.200
Sparse4D [21]	1600 \times 640	1	0.382	0.451	0.710	0.279	0.411	0.806	0.196
SimMOD [64]	1600 \times 900	1	0.366	0.455	0.698	0.264	0.340	0.784	0.197
DuoSpaceNet (Ours)	1600 \times 640	1	0.399	0.462	0.683	0.279	0.376	0.829	0.205
UVTR [15]	1600 \times 900	6	0.379	0.483	0.731	0.267	0.350	0.510	0.200
BEVFormer [18]	1600 \times 900	4	0.416	0.517	0.673	0.274	0.372	0.394	0.198
PETrv2 [27]	1600 \times 640	6	0.421	0.524	0.681	0.267	0.357	0.377	0.186
Sparse4D [21]	1600 \times 640	4	0.436	0.541	0.633	0.279	0.363	0.317	0.177
OCBEV [38]	1600 \times 900	4	0.417	0.532	0.629	0.273	0.339	0.342	0.187
DFA3D-MvACon [25]	1600 \times 900	4	0.432	0.535	0.664	0.275	0.344	0.323	0.207
DuoSpaceNet (Ours)	1600 \times 640	4	0.443	0.547	0.603	0.275	0.360	0.314	0.195

Table 1. Comparison on 3D detection results on nuScenes val set. All methods are trained for 24 epochs using ResNet-101-DCN [67] and benefit from perspective view pre-training. Test time augmentation is not used for all experiments.

Method	Space	Params	Flops	mAP \uparrow	NDS \uparrow
BEVDet	BEV	69.5M	1498.8G	0.339	0.389
BEVFormer-S	BEV	66.6M	1705.5G	0.375	0.448
Sparse4D $_{T=1}$	PV	58.3M	1453.8G	0.382	0.451
DuoSpaceNet	BEV+PV	64.8M	1771.7G	0.399	0.462

Table 2. Comparison on model complexity in terms of the number of parameters and the number of floating-point operations.

Method	Joint Training	IoU-Drivable \uparrow	IoU-Lane \uparrow
LSS	\times	72.9	20.0
M ² BEV	\checkmark	75.9	38.0
	\times	77.2	40.5
BEVFormer-S	\checkmark	77.6	19.8
	\times	80.7	21.3
DuoSpaceNet	\checkmark	80.8	45.9
(Ours)	\times	81.2	46.5

Table 3. Map segmentation on the nuScenes val set.

sion (mAP), nuScenes detection score (NDS), mean average error of translation (mATE), scale (mASE), orientation (mAOE), velocity (mAVE) and attribute (mAAE). For map segmentation, we follow previous works [37, 54] and evaluate our method with intersection of union (IoU) metric.

Implementation details. For both single-frame and multi-frame 3D detection experiments, unless specified otherwise, we follow the hyperparameter settings in [21], including learning rate and schedule, data augmentation, loss functions, and anchor initialization. For full model experiments, the BEV feature map is sized 200 \times 200, the number of duo space queries is 900 and the number of decoder layers is 4. All layers have identical settings with 8 attention heads in both self-attention and cross attention layers. For deformable cross attention layers, we compute 16 offsets per query. For multi-frame experiments, we use 4 adjacent frames (including the current frame) as temporal input. For all ablation studies, we use ResNet-50 [7], 100 \times 100 BEV feature map (if applicable), 800 \times 320 input images and a 2-layer decoder, trained for 12 epochs. For map segmentation, we follow PETrv2 [27] to transform map layers from the global reference frame into the ego frame, and generate two 200 \times 200 ground truth segmentation masks for *drivable area* and *lane boundary* respectively.

4.1. 3D Object Detection Results

Our 3D detection results on nuScenes val set are shown in Tab. 1. Compared with other state-of-the-art single-/multi-frame methods, our method consistently outperforms oth-

ers on mAP. Specifically, we achieve 1.7% mAP gain over the state-of-the-art PV-based method Sparse4D [21] and 2.4% mAP gain over the state-of-the-art BEV-based method BEVFormer-S [18], using the single-frame setup. The same is true for multi-frame results. Among all methods, DuoSpaceNet achieves the lowest mATE by a large margin, suggesting that our duo space design helps the model understand 3D scenes better. When it comes to other metrics, although our method does not achieve 1st place for some entries, we argue that on average our model surpasses others based on the NDS measurement. We also report our results on nuScenes test set in Tab. 4. Compared with PolarFormer-T [13], DuoSpaceNet achieves a considerable 1.2% mAP gain and 2.6% NDS gain. Note that different methods use different training strategies on the test set (e.g., longer training schedules, more temporal frames, etc.). Nonetheless, our model is capable of achieving competitive results against other state-of-the-art models.

We also compare our model complexity against other state-of-the-art BEV-only or PV-only methods using input images of size 1600 \times 640 under the single-frame setting. For all models, we test them on the same machine using DeepSpeed Flops Profiler¹. As shown in Tab. 2, under similar model sizes, DuoSpaceNet significantly outperforms BEVDet [10] and BEVFormer-S. It is also slightly better than Sparse4D, yet still capable of handling dense segmentation tasks.

¹<https://www.deepspeed.ai/tutorials/flops-profiler/>

Method	Temporal	Image Size	mAP \uparrow	NDS \uparrow	mATE \downarrow	mASE \downarrow	mAOE \downarrow	mAVE \downarrow	mAAE \downarrow
DETR3D [48]	✗	1600 \times 900	0.412	0.479	0.641	0.255	0.394	0.845	0.133
BEVDet [10]	✗	1600 \times 900	0.424	0.488	0.524	0.242	0.373	0.950	0.148
BEVFormer-S [18]	✗	1600 \times 900	0.435	0.495	0.589	0.254	0.402	0.842	0.131
PETR [26]	✗	1408 \times 512	0.441	0.504	0.593	0.249	0.383	0.808	0.132
PolarFormer [13]	✗	1600 \times 900	0.455	0.503	0.592	0.258	0.389	0.870	0.132
DuoSpaceNet (Ours)	✗	1600 \times 640	0.460	0.519	0.559	0.259	0.399	0.765	0.134
UVTR [15]	✓	1600 \times 900	0.472	0.551	0.577	0.253	0.391	0.508	0.123
BEVFormer [18]	✓	1600 \times 900	0.481	0.569	0.582	0.256	0.375	0.378	0.126
PETRv2 [27]	✓	1600 \times 640	0.490	0.582	0.561	0.243	0.361	0.343	0.120
PolarFormer-T [13]	✓	1600 \times 900	0.493	0.572	0.556	0.256	0.364	0.439	0.127
MV2D [49]	✓	1600 \times 900	0.511	0.596	0.525	0.243	0.357	0.357	0.120
Focal-PETR-T [45]	✓	1600 \times 640	0.511	0.592	0.546	0.243	0.373	0.357	0.115
DuoSpaceNet (Ours)	✓	1600 \times 640	0.513	0.601	0.508	0.254	0.362	0.312	0.118

Table 4. Comparison on 3D detection results on nuScenes test set. All experiments are camera-only methods using pretrained V2-99 [14] backbone. Test time augmentation is not used for all experiments.

Method	w/ BEV	w/ PV	mAP \uparrow	NDS \uparrow
BEV Only	✓		0.203	0.264
PV Only		✓	0.212	0.261
Duo (Ours)	✓	✓	0.216	0.288

Table 5. Ablation of using duo space features.

Method	FDE	mAP \uparrow	NDS \uparrow
BEV Only	✓	0.203	0.264
		0.210	0.260
Duo (Ours)	✓	0.216	0.288
		0.229	0.294

Table 6. Ablation of the proposed feature divergence enhancement, dubbed “FDE” in the table header.

Shared Pose	Shared Content	mAP \uparrow	NDS \uparrow
✓		0.202	0.252
✓	✓	0.225	0.290
		0.229	0.294

Table 7. Ablation of the proposed Duo Space Queries.

BEV Temporal Method	mAP \uparrow	NDS \uparrow
Recurrent Stacking	0.236	0.337
Learnable Attention	0.243	0.340
Temporal Queries	0.266	0.385

Table 8. Ablation of different temporal strategies.

4.2. Map Segmentation Results

In Tab. 3, we benchmark the map segmentation performance on nuScenes val set. All methods use ResNet-101-DCN backbone except for M²BEV, who has a more advanced backbone. Compared with previous methods, our model achieves the highest IoU for both *drivable area* and *lane boundary*, regardless of whether the segmentation branch is trained jointly with object detection or not. While sharing modules between different tasks saves computational resources and reduces inference time, the jointly trained model does show a slight performance drop compared to the individually trained model on map segmentation. This phenomenon, known as the negative transfer effect, is consistent with findings from previous studies [18].

4.3. Ablation Studies

Duo Space Features. To demonstrate the advantages of using BEV and PV features together, we compare the model equipped with our proposed duo space object queries to two baselines where object queries solely attend to either BEV or PV features. As shown in Tab. 5, using features from both spaces leads to a 0.4% gain in mAP from the PV-only baseline and a considerable 2.4% gain in NDS from the BEV-only baseline.

Feature Divergence Enhancement. To make BEV features more distinctive from PV features, we propose adding feature divergence enhancement (FDE) during BEV feature generation. As shown in Tab. 6, while adding it to the BEV-only baseline can improve mAP by 0.7%, it won’t yield any help on NDS. Adding FDE in conjunction with our duo

space design, however, will significantly improve the mAP by 1.3% and NDS by 0.6%, benefiting from the contrastiveness added between BEV and PV features.

Duo Space Queries. Although using feature maps from both spaces inherently has advantages over using those from a single space, optimal performance cannot be achieved without our delicately designed duo space object queries. To validate this, three models differing only in their decoders were obtained. The first model, “unshared pose and unshared content”, divides classical object queries into two sets, each attending separately to either BEV or PV features in cross-attention layers. The second model, “shared pose and shared content”, makes each classical object query sequentially pass through self-attention, PV and BEV cross-attention layers, thus sharing pose and content embedding across both spaces. The third model, “shared pose and un-

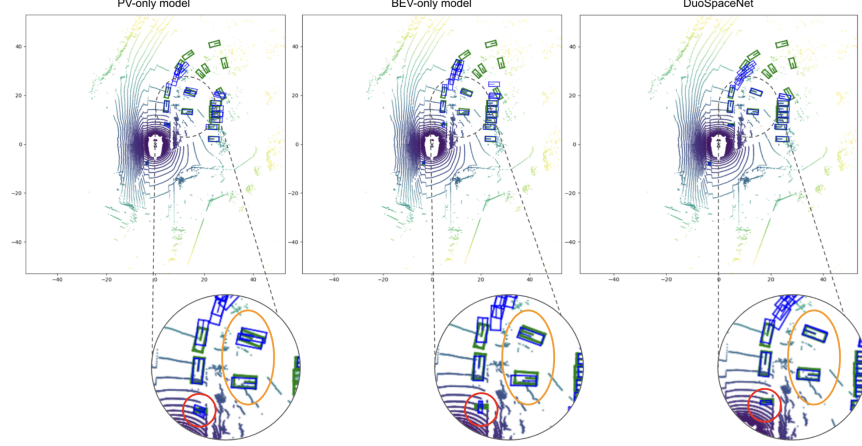


Figure 5. Qualitative comparison of top-down 3D detection results among our method, PV-only, and BEV-only models. Ground truth bounding boxes are in **green** and predictions are in **blue**. Our prediction aligns most accurately with the ground truth. Please refer to the supplementary materials for more visualization.

shared content”, is equipped with our proposed duo space object queries. As Tab. 7 reveals, the first setting yields the worst result. In such a setting, each query only sees a single space of features, thereby losing the potential advantages offered by the presence of duo space features. The performance is marginally improved when pose and content embeddings are both shared, while the best results are achieved coupled with our Duo Space Decoder design. This implies that directly sharing content features across spaces might create latent space confusion due to different feature distributions. Decoupling content embeddings, however, proves to be more optimal by preserving unique feature representations from both spaces.

Temporal Modeling. We demonstrate the necessity of a unified temporal solution for both spaces in contrast to some trivial solutions. We keep using temporal queries in PV space across all experiments. In each experiment, we use a different temporal strategy in BEV space. Specifically, “Recurrent Stacking” refers to infusing temporal information by stacking up temporal BEV features. “Learnable Attention” refers to infusing temporal information by temporal self-attention proposed in BEVFormer. “Temporal Queries” refers to our method where both spaces infuse temporal information into their temporal duo space queries. As clearly shown in Tab. 8, temporal strategy matters a lot. The proposed Duo Space Temporal Modeling achieves far superior performance compared with simply using other popular designs.

4.4. Qualitative Analysis

In addition to the quantitative analysis, we report qualitative results of our DuoSpaceNet in comparison with PV-only and BEV-only baselines. In this example, as top-down-view visualization (Fig. 5) reveals, the bounding boxes (highlighted by the **orange** ellipse) predicted by DuoSpaceNet

align more closely with the ground truth in 3D space compared to the PV-only baseline. This alignment is attributed to the more explicit 3D spatial information in BEV features. Regarding the object pose estimation (the **red** circle in Fig. 5, depicting a motorcycle in the real world), due to the significant appearance information in PV features, both DuoSpaceNet and the PV-only baseline accurately predict its heading angle. In contrast, the BEV-only baseline provides an erroneous prediction differing by 90 degrees from the ground truth. Combined, we are confident that our duo space paradigm achieves “the best of both world”.

5. Conclusion and Limitations

In this paper, we introduced DuoSpaceNet, a camera-based 3D perception framework that effectively integrates features from both BEV and PV spaces. The proposed duo-space decoder leverages dense BEV representations alongside detailed PV features, significantly enhancing performance on 3D object detection and map segmentation tasks. Extensive experiments on the nuScenes dataset demonstrate that DuoSpaceNet achieves competitive performance compared to state-of-the-art approaches, and ablation studies confirm the effectiveness of each proposed design. Our method can also benefit end-to-end self-driving [12, 43]. Beyond autonomous driving, our method holds potential for applications in human-centric tasks, such as human pose estimation [51, 52] and emotion understanding [44, 53].

Although our framework theoretically supports long-range 3D detection better than BEV-only methods, full evaluation is limited by insufficient far-range annotations in the nuScenes dataset. Future work will include comprehensive evaluations on larger datasets like Argoverse2 [50]. Additionally, current map segmentation relies exclusively on BEV features; integrating PV features could further enhance accuracy, particularly for detailed map structures.

References

- [1] Holger Caesar, Varun Bankiti, Alex H Lang, Sourabh Vora, Venice Erin Liong, Qiang Xu, Anush Krishnan, Yu Pan, Giancarlo Baldan, and Oscar Beijbom. nuscenes: A multi-modal dataset for autonomous driving. In *Proceedings of the IEEE/CVF conference on computer vision and pattern recognition*, pages 11621–11631, 2020. 2, 5, 1
- [2] Nicolas Carion, Francisco Massa, Gabriel Synnaeve, Nicolas Usunier, Alexander Kirillov, and Sergey Zagoruyko. End-to-end object detection with transformers. In *European conference on computer vision*, pages 213–229. Springer, 2020. 1
- [3] Yukang Chen, Jianhui Liu, Xiangyu Zhang, Xiaojuan Qi, and Jiaya Jia. Voxelnext: Fully sparse voxelnet for 3d object detection and tracking. In *Proceedings of the IEEE/CVF Conference on Computer Vision and Pattern Recognition*, pages 21674–21683, 2023. 1
- [4] Yiqian Gan, Hao Xiao, Yizhe Zhao, Ethan Zhang, Zhe Huang, Xin Ye, and Lingting Ge. Mgrt: Multi-granular transformer for motion prediction with lidar. *arXiv preprint arXiv:2312.02409*, 2023. 1
- [5] Chunrui Han, Jianjian Sun, Zheng Ge, Jinrong Yang, Runpei Dong, Hongyu Zhou, Weixin Mao, Yuang Peng, and Xiangyu Zhang. Exploring recurrent long-term temporal fusion for multi-view 3d perception. *arXiv preprint arXiv:2303.05970*, 2023. 1, 3
- [6] Adam W. Harley, Zhaoyuan Fang, Jie Li, Rares Ambrus, and Katerina Fragkiadaki. Simple-BEV: What really matters for multi-sensor bev perception? In *IEEE International Conference on Robotics and Automation (ICRA)*, 2023. 3, 4
- [7] Kaiming He, Xiangyu Zhang, Shaoqing Ren, and Jian Sun. Deep residual learning for image recognition. In *Proceedings of the IEEE conference on computer vision and pattern recognition*, pages 770–778, 2016. 3, 6
- [8] Yihan Hu, Jiazhi Yang, Li Chen, Keyu Li, Chonghao Sima, Xizhou Zhu, Siqi Chai, Senyao Du, Tianwei Lin, Wenhai Wang, Lewei Lu, Xiaosong Jia, Qiang Liu, Jifeng Dai, Yu Qiao, and Hongyang Li. Planning-oriented autonomous driving, 2023. 1
- [9] Junjie Huang and Guan Huang. Bevdet4d: Exploit temporal cues in multi-camera 3d object detection. *arXiv preprint arXiv:2203.17054*, 2021. 3, 5
- [10] Junjie Huang, Guan Huang, Zheng Zhu, and Dalong Du. Bevdet: High-performance multi-camera 3d object detection in bird-eye-view. *arXiv preprint arXiv:2112.11790*, 2021. 3, 6, 7
- [11] Peixiang Huang, Li Liu, Renrui Zhang, Song Zhang, Xinli Xu, Baichao Wang, and Guoyi Liu. Tig-bev: Multi-view bev 3d object detection via target inner-geometry learning. *arXiv preprint arXiv:2212.13979*, 2022. 1
- [12] Zhe Huang. *Distributed reinforcement learning for autonomous driving*. Carnegie Mellon University, 2022. 1, 8
- [13] Yanqin Jiang, Li Zhang, Zhenwei Miao, Xiatian Zhu, Jin Gao, Weiming Hu, and Yu-Gang Jiang. Polarformer: Multi-camera 3d object detection with polar transformer. In *Proceedings of the AAAI Conference on Artificial Intelligence*, pages 1042–1050, 2023. 6, 7
- [14] Youngwan Lee and Jongyoul Park. Centermask: Real-time anchor-free instance segmentation. In *Proceedings of the IEEE/CVF conference on computer vision and pattern recognition*, pages 13906–13915, 2020. 7
- [15] Yanwei Li, Yilun Chen, Xiaojuan Qi, Zeming Li, Jian Sun, and Jiaya Jia. Unifying voxel-based representation with transformer for 3d object detection. In *Advances in Neural Information Processing Systems*, pages 18442–18455. Curran Associates, Inc., 2022. 6, 7
- [16] Yinhao Li, Zheng Ge, Guanyi Yu, Jinrong Yang, Zengran Wang, Yukang Shi, Jianjian Sun, and Zeming Li. Bevdepth: Acquisition of reliable depth for multi-view 3d object detection. *Proceedings of the AAAI Conference on Artificial Intelligence*, 37(2):1477–1485, 2023. 3
- [17] Yanwei Li, Zhiding Yu, Jonah Philion, Anima Anandkumar, Sanja Fidler, Jiaya Jia, and Jose Alvarez. End-to-end 3d tracking with decoupled queries. In *Proceedings of the IEEE/CVF International Conference on Computer Vision*, pages 18302–18311, 2023. 1
- [18] Zhiqi Li, Wenhai Wang, Hongyang Li, Enze Xie, Chonghao Sima, Tong Lu, Qiao Yu, and Jifeng Dai. Bevformer: Learning bird’s-eye-view representation from multi-camera images via spatiotemporal transformers. *arXiv preprint arXiv:2203.17270*, 2022. 1, 3, 5, 6, 7
- [19] Tsung-Yi Lin, Piotr Dollár, Ross Girshick, Kaiming He, Bharath Hariharan, and Serge Belongie. Feature pyramid networks for object detection. In *Proceedings of the IEEE conference on computer vision and pattern recognition*, pages 2117–2125, 2017. 3, 4
- [20] Tsung-Yi Lin, Priya Goyal, Ross Girshick, Kaiming He, and Piotr Dollár. Focal loss for dense object detection. In *Proceedings of the IEEE international conference on computer vision*, pages 2980–2988, 2017. 5, 1
- [21] Xuewu Lin, Tianwei Lin, Zixiang Pei, Lichao Huang, and Zhizhong Su. Sparse4d: Multi-view 3d object detection with sparse spatial-temporal fusion. *arXiv preprint arXiv:2211.10581*, 2022. 1, 3, 4, 5, 6
- [22] Xuewu Lin, Tianwei Lin, Zixiang Pei, Lichao Huang, and Zhizhong Su. Sparse4d v2: Recurrent temporal fusion with sparse model. *arXiv preprint arXiv:2305.14018*, 2023. 1, 3
- [23] Xuewu Lin, Zixiang Pei, Tianwei Lin, Lichao Huang, and Zhizhong Su. Sparse4d v3: Advancing end-to-end 3d detection and tracking. *arXiv preprint arXiv:2311.11722*, 2023.
- [24] Haisong Liu, Yao Teng, Tao Lu, Haiguang Wang, and Limin Wang. Sparsebev: High-performance sparse 3d object detection from multi-camera videos. In *Proceedings of the IEEE/CVF International Conference on Computer Vision*, pages 18580–18590, 2023. 1, 3
- [25] Xianpeng Liu, Ce Zheng, Ming Qian, Nan Xue, Chen Chen, Zhebin Zhang, Chen Li, and Tianfu Wu. Multi-view attentive contextualization for multi-view 3d object detection. In *Proceedings of the IEEE/CVF Conference on Computer Vision and Pattern Recognition*, pages 16688–16698, 2024. 6
- [26] Yingfei Liu, Tiancai Wang, Xiangyu Zhang, and Jian Sun. Petr: Position embedding transformation for multi-view 3d object detection. In *Computer Vision – ECCV 2022*, pages 531–548, Cham, 2022. Springer Nature Switzerland. 2, 3, 6, 7

- [27] Yingfei Liu, Junjie Yan, Fan Jia, Shuailin Li, Aqi Gao, Tiancai Wang, and Xiangyu Zhang. Petrv2: A unified framework for 3d perception from multi-camera images. In *Proceedings of the IEEE/CVF International Conference on Computer Vision (ICCV)*, pages 3262–3272, 2023. 1, 3, 5, 6, 7
- [28] Yingfei Liu, Junjie Yan, Fan Jia, Shuailin Li, Aqi Gao, Tiancai Wang, and Xiangyu Zhang. Petrv2: A unified framework for 3d perception from multi-camera images. In *Proceedings of the IEEE/CVF International Conference on Computer Vision*, pages 3262–3272, 2023. 2, 3
- [29] Ilya Loshchilov and Frank Hutter. Sgdr: Stochastic gradient descent with warm restarts. *arXiv preprint arXiv:1608.03983*, 2016. 1
- [30] Ilya Loshchilov and Frank Hutter. Decoupled weight decay regularization. *arXiv preprint arXiv:1711.05101*, 2017. 1
- [31] Chenyang Lu, Marinus Jacobus Gerardus van de Molen-graft, and Gijs Dubbelman. Monocular semantic occupancy grid mapping with convolutional variational encoder-decoder networks. *IEEE Robotics and Automation Letters*, 4(2):445–452, 2019. 3
- [32] Fausto Milletari, Nassir Navab, and Seyed-Ahmad Ahmadi. V-net: Fully convolutional neural networks for volumetric medical image segmentation, 2016. 5
- [33] Bowen Pan, Jiankai Sun, Ho Yin Tiga Leung, Alex Andonian, and Bolei Zhou. Cross-view semantic segmentation for sensing surroundings. *IEEE Robotics and Automation Letters*, 5(3):4867–4873, 2020. 3
- [34] Jinhyung Park, Chenfeng Xu, Shijia Yang, Kurt Keutzer, Kris Kitani, Masayoshi Tomizuka, and Wei Zhan. Time will tell: New outlooks and a baseline for temporal multi-view 3d object detection. *arXiv preprint arXiv:2210.02443*, 2022. 3
- [35] Jinhyung Park, Chenfeng Xu, Shijia Yang, Kurt Keutzer, Kris Kitani, Masayoshi Tomizuka, and Wei Zhan. Time will tell: New outlooks and a baseline for temporal multi-view 3d object detection. *arXiv preprint arXiv:2210.02443*, 2022. 3
- [36] Lang Peng, Zhirong Chen, Zhangjie Fu, Pengpeng Liang, and Erkang Cheng. Bevsegformer: Bird’s eye view semantic segmentation from arbitrary camera rigs. In *Proceedings of the IEEE/CVF Winter Conference on Applications of Computer Vision*, pages 5935–5943, 2023. 3
- [37] Jonah Philion and Sanja Fidler. Lift, splat, shoot: Encoding images from arbitrary camera rigs by implicitly unprojecting to 3d. In *European Conference on Computer Vision*, pages 194–210. Springer, 2020. 3, 6
- [38] Zhangyang Qi, Jiaqi Wang, Xiaoyang Wu, and Hengshuang Zhao. Ocbbev: Object-centric bev transformer for multi-view 3d object detection. In *2024 International Conference on 3D Vision (3DV)*, pages 1188–1197. IEEE, 2024. 1, 3, 6
- [39] Olaf Ronneberger, Philipp Fischer, and Thomas Brox. U-net: Convolutional networks for biomedical image segmentation, 2015. 5
- [40] Carole H Sudre, Wenqi Li, Tom Vercauteren, Sebastien Ourselin, and M Jorge Cardoso. Generalised dice overlap as a deep learning loss function for highly unbalanced segmentations. In *Deep Learning in Medical Image Analysis and Multimodal Learning for Clinical Decision Support: Third International Workshop, DLMIA 2017, and 7th International Workshop, ML-CDS 2017, Held in Conjunction with MICCAI 2017, Québec City, QC, Canada, September 14, Proceedings 3*, pages 240–248. Springer, 2017. 1
- [41] Zheng Tang, Gaoang Wang, Hao Xiao, Aotian Zheng, and Jenq-Neng Hwang. Single-camera and inter-camera vehicle tracking and 3d speed estimation based on fusion of visual and semantic features. In *Proceedings of the IEEE conference on computer vision and pattern recognition workshops*, pages 108–115, 2018. 1
- [42] Ashish Vaswani, Noam Shazeer, Niki Parmar, Jakob Uszkoreit, Llion Jones, Aidan N Gomez, Łukasz Kaiser, and Illia Polosukhin. Attention is all you need. *Advances in neural information processing systems*, 30, 2017. 4
- [43] Adam R Villafior, Zhe Huang, Swapnil Pande, John M Dolan, and Jeff Schneider. Addressing optimism bias in sequence modeling for reinforcement learning. In *international conference on machine learning*, pages 22270–22283. PMLR, 2022. 8
- [44] James Z Wang, Sicheng Zhao, Chenyan Wu, Reginald B Adams, Michelle G Newman, Tal Shafir, and Rachelle Tsachor. Unlocking the emotional world of visual media: An overview of the science, research, and impact of understanding emotion. *Proceedings of the IEEE*, 111(10):1236–1286, 2023. 8
- [45] Shihao Wang, Xiaohui Jiang, and Ying Li. Focal-petr: Embracing foreground for efficient multi-camera 3d object detection. *IEEE Transactions on Intelligent Vehicles*, 2023. 7
- [46] Shihao Wang, Yingfei Liu, Tiancai Wang, Ying Li, and Xiangyu Zhang. Exploring object-centric temporal modeling for efficient multi-view 3d object detection. In *Proceedings of the IEEE/CVF international conference on computer vision*, pages 3621–3631, 2023. 3
- [47] Shihao Wang, Yingfei Liu, Tiancai Wang, Ying Li, and Xiangyu Zhang. Exploring object-centric temporal modeling for efficient multi-view 3d object detection. In *Proceedings of the IEEE/CVF International Conference on Computer Vision (ICCV)*, pages 3621–3631, 2023. 1, 3
- [48] Yue Wang, Guizilini Vitor Campagnolo, Tianyuan Zhang, Hang Zhao, and Justin Solomon. Detr3d: 3d object detection from multi-view images via 3d-to-2d queries. In *In Conference on Robot Learning*, pages 180–191, 2022. 1, 3, 6, 7
- [49] Zitian Wang, Zehao Huang, Jiahui Fu, Naiyan Wang, and Si Liu. Object as query: Lifting any 2d object detector to 3d detection. In *Proceedings of the IEEE/CVF International Conference on Computer Vision*, pages 3791–3800, 2023. 7
- [50] Benjamin Wilson, William Qi, Tanmay Agarwal, John Lambert, Jagjeet Singh, Siddhesh Khandelwal, Bowen Pan, Ratnesh Kumar, Andrew Hartnett, Jhony Kaesemodel Pontes, Deva Ramanan, Peter Carr, and James Hays. Argoverse 2: Next generation datasets for self-driving perception and forecasting. In *Proceedings of the Neural Information Processing Systems Track on Datasets and Benchmarks (NeurIPS Datasets and Benchmarks 2021)*, 2021. 8
- [51] Chenyan Wu, Yukun Chen, Jiajia Luo, Che-Chun Su, Anuja Dawane, Bikramjot Hanzra, Zhuo Deng, Bilan Liu, James Z Wang, and Cheng-hao Kuo. Mebow: Monocular estimation of body orientation in the wild. In *Proceedings of*

- the *IEEE/CVF Conference on Computer Vision and Pattern Recognition*, pages 3451–3461, 2020. 8
- [52] Chenyan Wu, Yandong Li, Xianfeng Tang, and James Wang. Mug: Multi-human graph network for 3d mesh reconstruction from 2d pose. *arXiv preprint arXiv:2205.12583*, 2022. 8
- [53] Chenyan Wu, Dolzodmaa Davaasuren, Tal Shafir, Rachelle Tsachor, and James Z Wang. Bodily expressed emotion understanding through integrating laban movement analysis. *Patterns*, 4(10), 2023. 8
- [54] Enze Xie, Zhiding Yu, Daquan Zhou, Jonah Philion, Anima Anandkumar, Sanja Fidler, Ping Luo, and Jose M. Alvarez. M²bev: Multi-camera joint 3d detection and segmentation with unified birds-eye view representation, 2022. 1, 3, 6
- [55] Kaixin Xiong, Shi Gong, Xiaoqing Ye, Xiao Tan, Ji Wan, Errui Ding, Jingdong Wang, and Xiang Bai. Cape: Camera view position embedding for multi-view 3d object detection. In *Proceedings of the IEEE/CVF Conference on Computer Vision and Pattern Recognition (CVPR)*, pages 21570–21579, 2023. 3
- [56] Chenyu Yang, Yuntao Chen, Hao Tian, Chenxin Tao, Xizhou Zhu, Zhaoxiang Zhang, Gao Huang, Hongyang Li, Yu Qiao, Lewei Lu, Jie Zhou, and Jifeng Dai. Bevformer v2: Adapting modern image backbones to bird’s-eye-view recognition via perspective supervision. In *Proceedings of the IEEE/CVF Conference on Computer Vision and Pattern Recognition (CVPR)*, pages 17830–17839, 2023. 1, 3
- [57] Chenyu Yang, Yuntao Chen, Hao Tian, Chenxin Tao, Xizhou Zhu, Zhaoxiang Zhang, Gao Huang, Hongyang Li, Yu Qiao, Lewei Lu, et al. Bevformer v2: Adapting modern image backbones to bird’s-eye-view recognition via perspective supervision. In *Proceedings of the IEEE/CVF Conference on Computer Vision and Pattern Recognition*, pages 17830–17839, 2023. 2, 3
- [58] Dongqiangzi Ye, Zixiang Zhou, Weijia Chen, Yufei Xie, Yu Wang, Panqu Wang, and Hassan Foroosh. Lidarmultinet: Towards a unified multi-task network for lidar perception. In *Proceedings of the AAAI Conference on Artificial Intelligence*, pages 3231–3240, 2023. 1
- [59] Tianwei Yin, Xingyi Zhou, and Philipp Krahenbuhl. Center-based 3d object detection and tracking. In *Proceedings of the IEEE/CVF conference on computer vision and pattern recognition*, pages 11784–11793, 2021. 1
- [60] Rui Yu and Zihan Zhou. Towards robust human trajectory prediction in raw videos. In *2021 IEEE/RSJ International Conference on Intelligent Robots and Systems (IROS)*, pages 8059–8066. IEEE, 2021. 1
- [61] Rui Yu, Zhenyuan Yuan, Minghui Zhu, and Zihan Zhou. Data-driven distributed state estimation and behavior modeling in sensor networks. In *2020 IEEE/RSJ International Conference on Intelligent Robots and Systems (IROS)*, pages 8192–8199. IEEE, 2020. 1
- [62] Weijiang Yu, Zhe Huang, Wayne Zhang, Litong Feng, and Nong Xiao. Gradual network for single image de-raining. In *Proceedings of the 27th ACM international conference on multimedia*, pages 1795–1804, 2019. 1
- [63] Ethan Zhang, Hao Xiao, Yiqian Gan, and Lei Wang. Sapi: Surroundings-aware vehicle trajectory prediction at intersections. *arXiv preprint arXiv:2306.01812*, 2023. 1
- [64] Yunpeng Zhang, Wenzhao Zheng, Zheng Zhu, Guan Huang, Jiwen Lu, and Jie Zhou. A simple baseline for multi-camera 3d object detection. In *Proceedings of the AAAI Conference on Artificial Intelligence*, pages 3507–3515, 2023. 6
- [65] Brady Zhou and Philipp Krähenbühl. Cross-view transformers for real-time map-view semantic segmentation. *arXiv preprint arXiv:2205.02833*, 2022. 3
- [66] Yin Zhou, Pei Sun, Yu Zhang, Dragomir Anguelov, Jiyang Gao, Tom Ouyang, James Guo, Jiquan Ngiam, and Vijay Vasudevan. End-to-end multi-view fusion for 3d object detection in lidar point clouds. In *Conference on Robot Learning*, pages 923–932. PMLR, 2020. 3
- [67] Xizhou Zhu, Han Hu, Stephen Lin, and Jifeng Dai. Deformable convnets v2: More deformable, better results, 2018. 6
- [68] Xizhou Zhu, Weijie Su, Lewei Lu, Bin Li, Xiaogang Wang, and Jifeng Dai. Deformable detr: Deformable transformers for end-to-end object detection. *arXiv preprint arXiv:2010.04159*, 2020. 3, 4, 5, 2
- [69] Zhuofan Zong, Dongzhi Jiang, Guanglu Song, Zeyue Xue, Jingyong Su, Hongsheng Li, and Yu Liu. Temporal enhanced training of multi-view 3d object detector via historical object prediction. In *Proceedings of the IEEE/CVF International Conference on Computer Vision (ICCV)*, pages 3781–3790, 2023. 3

DuoSpaceNet: Leveraging Both Bird’s-Eye-View and Perspective View Representations for 3D Object Detection

Supplementary Material

6. Additional details on Duo Space Temporal Modeling.

Specifically, we generate temporal duo space queries $\mathbf{z}_{BEV}^{(t)}$ and $\mathbf{z}_{PV}^{(t)}$ by infusing past information into shared 3D poses. Assuming the current timestamp is T and the temporal length is l frames, we compute temporal poses $\mathcal{P}_i^{(t)}, i \in \{1, 2, \dots, k\}, t \in \{T-l+1, T-l+2, \dots, T\}$. Ego-motion compensation can be done via a warp transformation matrix from timestamp $t-1$ to t , denoted as $[\mathbf{R}|\mathbf{t}]_{(t)}^{(t-1)}, t \in \{T-l+1, T-l+2, \dots, T\}$, where \mathbf{R} and \mathbf{t} refer to the rotational and translational components in the matrix. Object-motion compensation, on the other hand, can be tackled using the predicted velocity of each query, assuming a constant velocity motion model over the l -length sequence. Adding up both compensations, we update the object location x, y, z at $t-1$, dubbed $\mathcal{P}_i^{(t-1)}|_{x,y,z}$, the object orientation $\sin \theta, \cos \theta$ at $t-1$, dubbed $\mathcal{P}_i^{(t-1)}|_{\theta}$ and the object velocity vx, vy at $t-1$, dubbed $\mathcal{P}_i^{(t-1)}|_{vx,vy}$, through

$$\mathcal{P}_i^{(t)}|_{x',y'} = \mathcal{P}_i^{(t)}|_{x,y} - \Delta t \cdot \mathcal{P}_i^{(t)}|_{vx,vy}, \quad (10)$$

$$\mathcal{P}_i^{(t-1)}|_{x,y,z} = [\mathbf{R}|\mathbf{t}]_{(t)}^{(t-1)} \mathcal{P}_i^{(t)}|_{x',y',z}, \quad (11)$$

$$\mathcal{P}_i^{(t-1)}|_{\theta} = \mathbf{R}_{(t)}^{(t-1)} \mathcal{P}_i^{(t)}|_{\theta}, \quad (12)$$

$$\mathcal{P}_i^{(t-1)}|_{vx,vy} = \mathbf{R}_{(t)}^{(t-1)} \mathcal{P}_i^{(t)}|_{vx,vy}, \quad (13)$$

$$i \in \{1, 2, \dots, k\}, t \in \{T-l+1, T-l+2, \dots, T\},$$

where Δt represents the wall-clock time difference between adjacent frames. We compute the temporal pose embedding for each timestamp t as follows:

$$(Q_{Pose}^i)^{(t)} = \xi \left(\text{Enc}(\mathcal{P}_i^{(t)}) \right). \quad (14)$$

We then generate $\mathbf{z}_{BEV}^{(t)}, \mathbf{z}_{PV}^{(t)}, \hat{\mathbf{p}}_{BEV}^{(t)}$ and $\hat{\mathbf{p}}_{PV}^{(t)}, t \in \{T-l+1, T-l+2, \dots, T\}$ according to Eq. 2, 3, 6 & 8 as temporal inputs. Finally, after cross-attention layers (Eq. 7 and 9), we aggregate temporal outputs via 3-layer MLP before the FFN of each decoder layer. An illustration of temporal cross-attention in PV space is shown in Fig. 6. The temporal cross-attention in BEV space is identical except for the use of BEV space queries and BEV features as input.

7. Additional details on experiment settings.

Following [21], we initialize the x, y, z coordinates of pose vectors using K-Means centroids on nuScenes training

set [1]. For all experiments, we use AdamW optimizer [30] and a cosine learning rate scheduler [29]. The initial learning rate for backbone and other modules are $2e-5$ and $2e-4$, respectively. No data augmentation is used other than the grid mask used in DETR3D [48]. The perception ranges for both the X and Y axes are $[-51.2m, 51.2m]$, which are consistent for both the 3D object detection and map segmentation tasks.

When it comes to the loss functions we use to train the 3D detection, we utilize Focal Loss [20] for bounding box classification and L1 Loss for attribute regression. Duo space queries are assigned to their ground truth via Hungarian Matching introduced in DETR [2]. For segmentation, we use a combination of L1 Loss, Cross Entropy Loss and Dice Loss [40] for each predicted mask.

8. Additional Visualizations

In Fig. 7, the 3D detection results are displayed in the perspective camera view for the same example as shown in Fig. 5, comparing three different detection methods along with the ground truth.

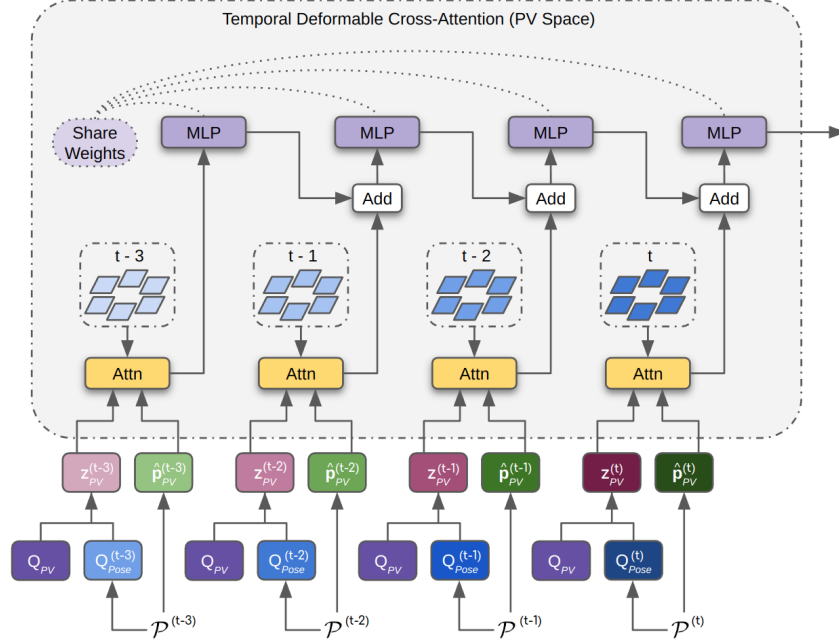


Figure 6. An illustration of space-specific temporal deformable cross-attention in perspective view (PV) space, with 4 temporal frames. Temporal pose vectors are generated by transforming current the pose vector at current frame to previous frames with motion compensation. After the duo space query composition, duo space temporal queries are formulated for both spaces. Subsequently, in PV space, attention queries, $\mathbf{z}_{PV}^{(\cdot)}$, and their reference points, $\hat{\mathbf{p}}_{PV}^{(\cdot)}$, from timestamp $t-3$ to t are used as input queries for multi-scale deformable attention [68]. Each set of queries at a given timestamp only attends to corresponding PV features at the same timestamp. After the attention mechanism, results are aggregated by MLPs in a recurrent manner. Note that weights are shared across all MLPs.



Figure 7. Visualization of 3D detection results in perspective camera view. Different colors represent different categories. Our method achieves the best prediction result for the motorcycle instance w.r.t. its 3D position as well as its orientation, showcasing the effectiveness of incorporating both PV and BEV information in detection queries.